

# An Assessment of Coupled Inductor Modeling for a Multi-output Flyback Converter

F. Farahmand,<sup>\*</sup> F. P. Dawson,<sup>†</sup> J. D. Lavers<sup>‡</sup>

The Edward S. Rogers Sr. Department of Electrical and Computer Engineering  
University of Toronto, 10 King's College Road, Toronto, Ontario, M5S 3G4, Canada  
Email: <sup>\*</sup>f.farahmand@utoronto.ca, <sup>†</sup>dawson@ele.utoronto.ca, <sup>‡</sup>doug.lavers@utoronto.ca

**Abstract**—In this paper, simulation results for a five-winding coupled inductor in a multi-output flyback converter are compared with experimental results. The simulations were usually aborted due to numerical convergence problems. This has been overcome by rearranging the elements of the equivalent circuit of the coupled inductor so as to place every inductance in series with a resistance. Discrepancies between the simulation and experiment have been categorized as follows: (i) coupling factors significantly influence the shapes of the secondary current waveforms and steepness of the slope after a switch transition; (ii) the representations of winding and core losses affect only the losses and not the shapes of the waveforms; (iii) the magnetizing inductance determines whether the converter operates in the continuous or discontinuous current mode.

## I. INTRODUCTION

Although circuit simulators such as PSpice are readily available for simulating a flyback converter, the first step for their use is to have appropriate models for the components used in the converter, in particular the coupled inductor. Modeling the coupled inductor in a single-output flyback converter using only the magnetizing inductance and an ideal transformer (which is equivalent to perfectly coupled inductances) suffices from the standpoint of predicting the main features of the waveforms. However for a multi-output flyback converter, a more comprehensive model of the coupled inductor should be used in order to obtain better agreement between the simulation and experimental results.

In previous research [1], simulation results of two coupled inductor equivalent circuits were compared with experimental waveforms for a triple-output flyback converter. One of the equivalent circuits referred to in [1] is denoted as a full-order extended cantilever network. This network consists of ideal transformers for secondary windings which are interconnected to themselves and to the primary winding through leakage inductances. Additionally, the primary has a shunt self inductance. The second circuit is the reduced-order ladder network in which the leakage inductances between non-adjacent windings are deleted from the full-order network. The results presented in [1] have shown that none of the above models provide agreement between the simulated and experimental secondary current waveforms.

A more detailed equivalent circuit for a coupled inductor can be obtained using the finite-element-method based software package PEmag [2]. PEmag was developed based on the formulation described in [3]. The equivalent circuit

obtained by PEmag includes perfectly coupled inductances. In addition, leakages and high frequency effects are taken into account by using frequency-dependent RL impedances for each winding and between every combination of winding pair. These frequency-dependent impedances are obtained using finite element analyses and are approximated using Foster networks.

In the present paper, we show that even with the PEmag circuit, the simulated secondary current waveforms are not in close agreement with the experiment. In addition, the shunt inductances in the Foster networks contribute to numerical divergence in PSpice simulations. To overcome this problem, the PSpice documentation suggests that every inductance should be placed in series with a resistance.

This paper proposes a method for generating an alternative circuit of the PEmag model to resolve the convergence problem. The parallel RL combinations in the Foster networks are reconfigured as individual first order series RL networks which interact with the main circuit through current controlled voltage sources (CCVS). The series inductances of the Foster networks, on the other hand, are combined with the perfectly coupled inductances to form coupled inductances with coupling factors that are less than one.

The effects of the model parameters on the waveforms, loss and converter current mode of operation are also studied. The model parameters considered include representations of core and winding losses (core hysteresis and winding resistances), coupling factors and magnetizing inductance.

## II. COUPLED INDUCTOR MODELING

The software package PEmag is used to model the coupled inductor being used in this study for high frequencies. This package provides an equivalent circuit similar to the one presented in [3]. Fig. 1 shows how a two winding device is modeled. The windings are represented by perfectly coupled inductances, i.e.  $L_1$  and  $L_2$  with a coupling factor of  $k = 1$ . Additionally, each winding has a frequency-dependent leakage impedance, i.e.  $Z_{11}$  and  $Z_{22}$ , and every combination of winding pairs has a frequency-dependent mutual impedance, i.e.  $Z_{12}$ .

The frequency-dependent impedances are implemented using the series Foster networks shown in Fig. 2. To compute the parameters of the Foster networks, first, PEmag obtains a 2-D

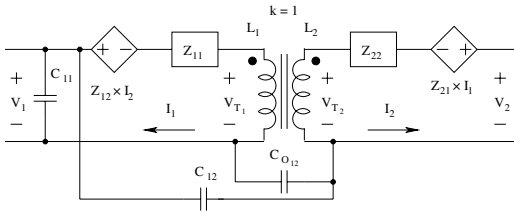


Fig. 1. PEmag equivalent circuit for a two winding component

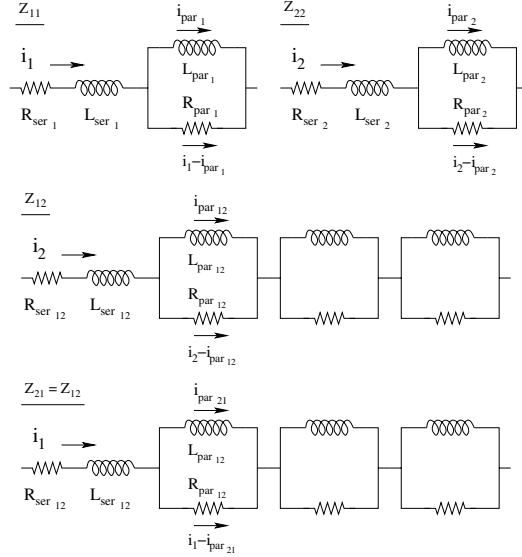


Fig. 2. PEmag equivalent circuit for a two winding component

axisymmetric equivalent representation of the magnetic component [3], if it is 3-D. Then the quasi-static magnetic Finite Element Method is used to calculate the open circuit frequency responses of the 2-D equivalent magnetic component over a frequency range that the user has defined. Finally, each Foster network in Fig. 2 is fitted to the respective frequency response by minimizing the least means square error.

Capacitive effects between the turns of the windings can be important for very high frequencies. To obtain the frequency responses, PEmag assumes that the displacement currents are negligible. Therefore these capacitive effects are ignored. They are partly compensated using lumped capacitors between the terminals of the windings as illustrated in Fig. 1 [4]. The lumped capacitors are computed using an electrostatic Finite Element Method. For the magnetic component studied in this paper, these capacitors are on the order of several pico farads and for our flyback case study, with a 40 kHz switching frequency, the simulations show no obvious differences in the waveforms if the capacitances are eliminated from the equivalent network.

Utilizing a 2-D equivalent magnetic component instead of a 3-D component introduces errors in the frequency responses that are estimated to be no greater than 25% [5]. There are also errors in fitting the Foster networks to the frequency responses. In particular, a shortcoming of PEmag is that the orders of the Foster networks are fixed and cannot be changed. Therefore,

the use of a wider range of frequency can result in larger errors when the networks are fitted to the frequency responses. As an example, the fitting errors for our case study increase by 10% from 5–20% to 15–30% when the range of frequencies increases from 0–1 MHz to 0–2 MHz.

The model previously described assumes a linear lossless core. To include the core loss in the equivalent circuit, one can consider an equivalent resistance in parallel with  $L_1$ . However, the value of the resistance is a function of operating voltage and frequency and should be recomputed using approaches such as those proposed in [6], [7] or [8] if the operating point changes.

Alternatively, it is possible to include the Jiles–Atherton (J–A) nonlinear core representation [9] in the circuit. In this way, PSpice simultaneously incorporates the B–H loop along with currents and voltages. An advantage of this method is that the core loss and impacts of a nonlinear core on waveforms are taken into account inherently. However, numerical convergence problems are far more severe than the lossless core model or a model that introduces losses in the form of a fixed resistance.

PSpice simulations using the equivalent circuits given by PEmag usually exhibit numerical divergence. PSpice produces error messages that primarily refer to the shunt inductances of the Foster networks used in modeling the coupled inductor as potential sources of the convergence problem. The PSpice documentation recommends that every inductance be placed in series with a resistance. Therefore to resolve the convergence problem, the PEmag network is reconfigured in the form of another circuit model which is described next.

#### A. Alternative network for a two winding component

The equivalent network topology shown in Fig. 1 and Fig. 2 is used to show the method of extracting the alternative network from a PEmag circuit. For simplicity, only one parallel RL branch is taken into account for each Foster network in Fig. 2. Also, no capacitance effects are considered. The results are extended in the next subsection for a general PEmag circuit with any number of windings and parallel branches.

First, Kirchhoff's Voltage Law (KVL) is applied to the primary side to obtain (1).

$$v_1 = L_{ser1} \dot{i}_1 + R_{ser1} i_1 + R_{par1} (i_1 - i_{par1}) + L_{ser12} \dot{i}_2 + R_{ser12} i_2 + R_{par12} (i_2 - i_{par12}) + v_{T1} \quad (1)$$

Substituting the coupled inductance characteristic equation, i.e. (2), into (1) results in (3).

$$v_{T1} = L_1 \times \dot{i}_1 + \sqrt{L_1 L_2} \times \dot{i}_2 \quad (2)$$

$$v_1 = (L_1 + L_{ser1}) \dot{i}_1 + \left( \sqrt{L_1 L_2} + L_{ser12} \right) \dot{i}_2 + (R_{ser1} + R_{par1}) i_1 - R_{par1} i_{par1} + (R_{ser12} + R_{par12}) i_2 - R_{par12} i_{par12} \quad (3)$$

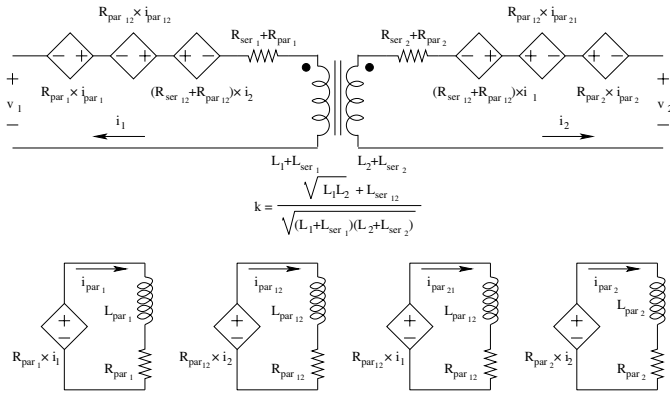


Fig. 3. Alternative circuit for Fig. 1 considering only one shunt RL loop for the Foster network

Equation (4) is obtained by applying a similar KVL for the secondary side.

$$\begin{aligned}
 v_2 = & (L_2 + L_{ser2}) \dot{i}_2 + (\sqrt{L_1 L_2} + L_{ser12}) \dot{i}_1 \\
 & + (R_{ser2} + R_{par2}) i_2 - R_{par2} i_{par2} \\
 & + (R_{ser12} + R_{par12}) i_2 - R_{par12} i_{par21}
 \end{aligned} \quad (4)$$

The KVL's inside the loops of the parallel RL combinations, i.e. (5), provide governing equations for the remaining inductances.

$$\begin{cases}
 L_{par1} \dot{i}_{par1} - R_{par1} (i_1 - i_{par1}) = 0 \\
 L_{par12} \dot{i}_{par12} - R_{par12} (i_2 - i_{par12}) = 0 \\
 L_{par2} \dot{i}_{par2} - R_{par2} (i_2 - i_{par2}) = 0 \\
 L_{par12} \dot{i}_{par21} - R_{par12} (i_1 - i_{par21}) = 0
 \end{cases} \quad (5)$$

Finally, a rearranged format of the above equation, which is shown in (6), along with (3) and (4) is used to generate the alternative equivalent network for the magnetic component as shown Fig. 3.

$$\begin{cases}
 L_{par1} \dot{i}_{par1} + R_{par1} i_{par1} = R_{par1} i_1 \\
 L_{par12} \dot{i}_{par12} + R_{par12} i_{par12} = R_{par12} i_2 \\
 L_{par2} \dot{i}_{par2} + R_{par2} i_{par2} = R_{par2} i_2 \\
 L_{par12} \dot{i}_{par21} + R_{par12} i_{par21} = R_{par12} i_1
 \end{cases} \quad (6)$$

In summary, with reference to Fig. 3, the series inductances  $L_{ser1}$ ,  $L_{ser2}$  and  $L_{ser12}$  in the Foster networks and the perfectly coupled inductances  $L_1$  and  $L_2$  are integrated to form coupled inductances with a coupling factor that is less than 1. The shunt inductances in the Foster networks,  $L_{par1}$ ,  $L_{par12}$  and  $L_{par2}$ , form separate subnetworks which are linked to the main circuit by current controlled voltage sources (CCVS). The transresistance of each of the CCVS's equals the shunt resistance of the respective RL loop. For each winding, there is an additional CCVS which is controlled by the other winding's current and has a transresistance that equals the sum of all the resistances in the mutual Foster network  $Z_{12}$ . In addition, all of the resistances in the impedances  $Z_{11}$  and  $Z_{22}$  appear as series resistances for the primary and secondary circuits respectively.

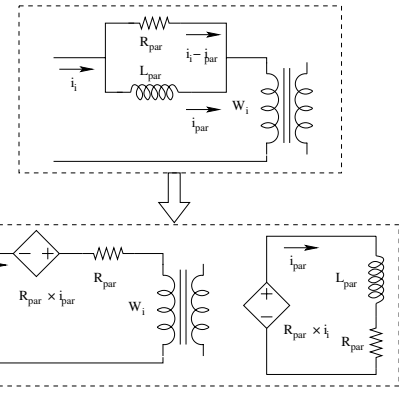


Fig. 4. Alternative network for a shunt RL in self impedances

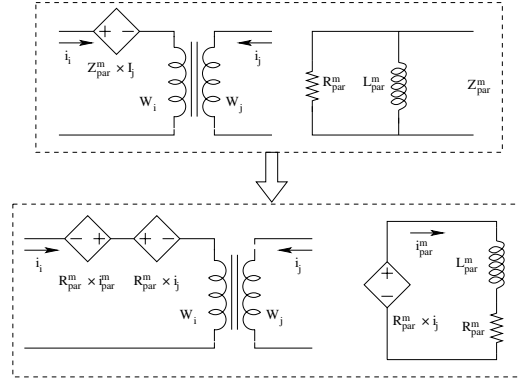


Fig. 5. Alternative network for a shunt RL in mutual impedances

## B. General procedure to generate alternative network

Based on the previous subsection, the following procedure is proposed to generate the alternative network for any PEmag circuit:

- 1) Delete all  $L_{ser}$ 's and replace every  $L_i$  of the perfectly coupled inductances with  $L_i + L_{seri}$
- 2) Change the coupling factor between coupled inductances  $i$  and  $j$  from 1 to

$$k_{ij} = \frac{(\sqrt{L_i L_j} + L_{serij})}{\sqrt{(L_i + L_{seri}) \times (L_j + L_{serj})}}. \quad (7)$$

- 3) Reconfigure each parallel RL branch in the  $i$ th self impedance as shown in Fig. 4. Each RL loop is replaced with a series resistance and a reversed-polarity CCVS, and a separate series RL circuit which is supplied by another CCVS. The transresistances of the CCVS's are equal to the respective loop's resistance.
- 4) Reconfigure each parallel RL branch in the mutual impedance between windings  $i$  and  $j$  as shown in Fig. 5. The procedure is similar to the one shown in Fig. 4 with the exception that the series resistance is replaced with another CCVS.
- 5) Leave all of the  $R_{ser}$ 's as they are.

### C. Alternative network with J–A core representation

For a network that includes a nonlinear J–A core representation, no coupling factor can be defined using (7) since the coupled inductances, e.g.  $L_1$  and  $L_2$ , are replaced with the turn numbers of the windings and parameters to define the B–H loop of the core. A method to work around this problem is to use the coupling factors obtained for the linearized network. However, only one global coupling factor for all winding pairs has to be specified in PSpice if the J–A core model is used. Therefore for a triple– or higher–winding magnetic component, items 1 and 2 in the procedure described in section II–B, should not be considered and only the parallel RL combinations are reconfigured.

### D. Advantages of proposed formulation

The alternative circuit results in shorter simulation run times since the new formulation allows for larger time steps. As an example, for our case study, the simulation with the alternative circuit was about two times faster than that with the PEmag circuit. Alternatively, solutions can be obtained with better accuracies using smaller error tolerances. For example for our case study, with respect to the PEmag circuit, the absolute current error tolerance for the alternative circuit simulation could be lowered by a factor of 100 from 10 nA to 0.1 nA while the simulation run times for the original lossless core circuit and the alternative circuit were approximately the same. An absolute current error tolerance lower than 10 nA resulted in divergence for the simulation with the PEmag circuit.

## III. COMPARISON OF SIMULATION AND EXPERIMENTAL RESULTS

The triple–output flyback converter shown in Fig. 6 has been studied. The converter has a 14 V output and two 5 V outputs. One of the 5 V outputs is connected to a regulator. The other 5 V output and the 14 V output are connected to a tapped winding and are controlled by a PWM controller. An extra secondary winding is included in order to power the PWM controller.

In our experiments, the resistive loads,  $R_{L3}$ ,  $R_{L4}$  and  $R_{L5}$ , are set such that their measured currents are 500, 700 and 500 mA respectively. The experimental waveforms were logged in files using a Tektronix TDS3014 oscilloscope. The current waveforms were obtained using a Tektronix A6312 current probe. The switching frequency is approximately 40 kHz with a duty cycle of about 14%.

Two equivalent circuits for the five–winding coupled inductor are obtained using PEmag: one with a lossless linear core and the other one with the J–A model of the core. Their Foster networks are optimized for a frequency range from DC to 1 MHz. The fitting errors range from 5 to 20%. To resolve convergence problems, the alternative circuits of the networks are used instead of the PEmag circuits. We have also simulated another equivalent circuit in which the core loss is taken into account using an equivalent shunt resistance. The value of the resistance was calculated to be about 5 k $\Omega$  using the primary voltage waveforms and computed core loss from the equivalent

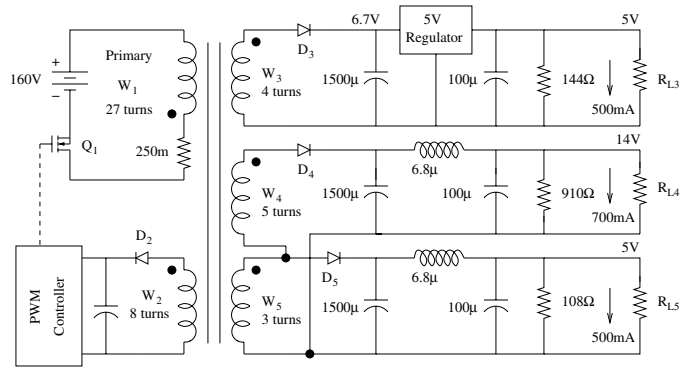
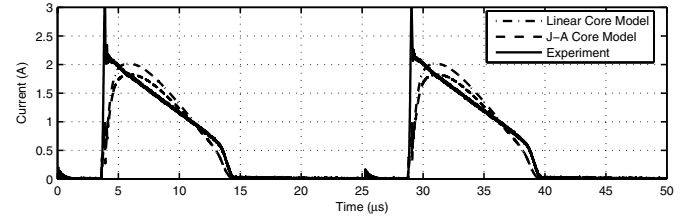
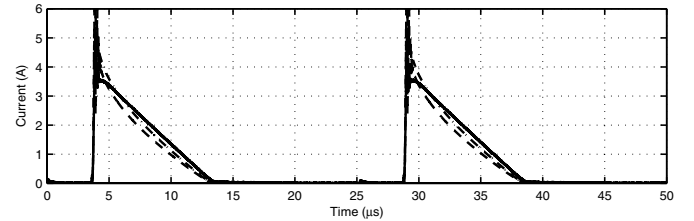


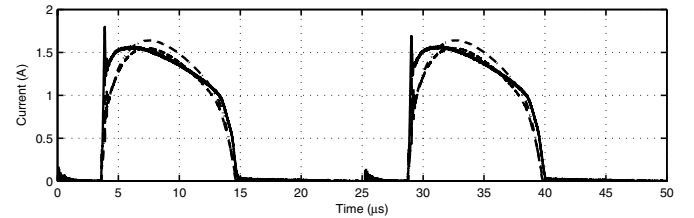
Fig. 6. Triple-output flyback converter



(a)  $D_3$  current



(b)  $D_4$  current



(c)  $D_5$  current

Fig. 7. Experimental and simulated current waveforms

circuit with the J–A core model. The simulation shows that the existence of the equivalent shunt resistance does not cause any visible change to the waveforms with respect to those of the lossless core circuit without the shunt resistance. Hence, no further study is carried out on this type of equivalent circuit.

Fig. 7 compares the simulated and experimental waveforms for the currents of the secondary diodes. This figure illustrates that the equivalent circuits provided by PEmag cannot accurately replicate the secondary current waveforms. In particular, there are large differences in the rise times of the currents at a switching transition.

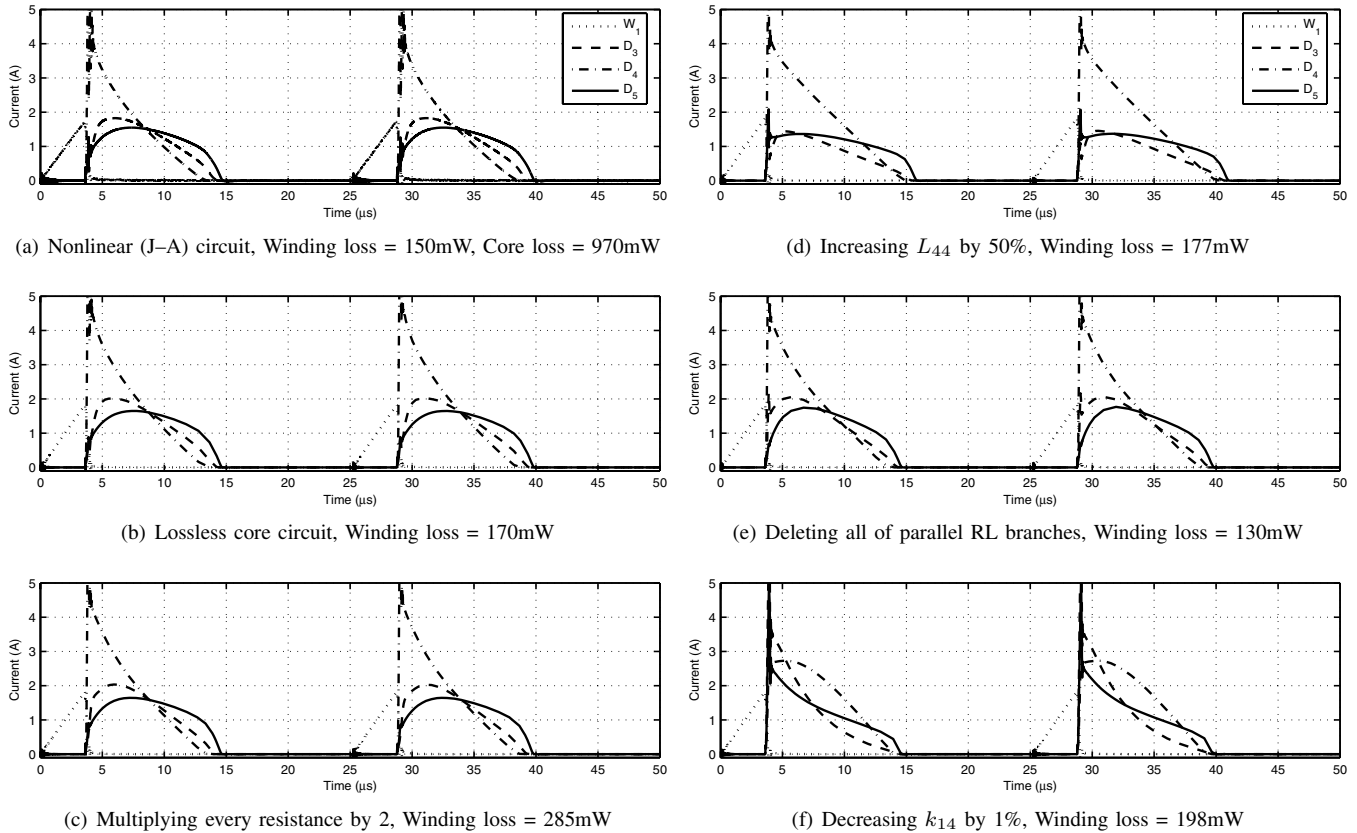


Fig. 8. Effects of changing parameters on simulated current waveforms

#### IV. EFFECTS OF EQUIVALENT NETWORK PARAMETERS

To understand the reasons for the discrepancies between the simulated and experimental waveforms, the effects of the equivalent circuit parameters on the waveforms are studied and compared in Fig. 8.

##### A. Winding and core losses

First of all, as Fig. 8(a) and Fig. 8(b) show, the use of a lossless model for the core or a J–A core model does not significantly affect the shapes of the simulated waveforms. However, they have impacts on the total loss. With the linear lossless core model, the winding loss is estimated to be about 170 mW. The Modified Steinmetz Equation (MSE) method [7] is used to estimate the core loss from the simulated magnetizing current. The MSE method is an adaptation of the empirical Steinmetz equation for a nonsinusoidal magnetizing current. The core loss estimate using the MSE method is on the order of 590–685 mW. The network with the J–A model, on the other hand, predicts a 150 mW winding loss and a 970 mW core loss. The large difference in the core loss estimates can arise for the following reasons: (i) there are unavoidable mismatches between the B–H loop of the J–A core model and that of the datasheets; (ii) the temperature dependency of the B–H loop cannot be taken into account in the J–A core model.

The numerical calculation of the winding loss is sensitive to the maximum time step that is defined for PSpice. For the values noted in Fig. 8, the maximum time step was set to 1 ns. If the maximum time step is increased to 1000 ns, although the waveforms seem exactly the same, there is a 30% rise in the winding loss. The winding loss is calculated by time averaging the instantaneous products of voltages and currents of the resistances. Therefore, the error in calculating the winding loss is due to poor time averaging for larger time steps.

A comparison of the results in Fig. 8(b), Fig. 8(d) and Fig. 8(f) shows that the winding loss is not dependent on the values of the inductances and coupling factors.

##### B. Flyback current mode of operation

Fig. 7 and Fig. 8 illustrate that despite differences in the waveform shapes, all of the circuits can predict that the flyback converter operates in the discontinuous current mode. Moreover, they all agree with the experiment in terms of the secondary conduction time period. Therefore, the values of the coupling factors, J–A parameters and resistances in the equivalent circuit have no significant impact on the boundary between continuous and discontinuous current modes of operation. The boundary between continuous and discontinuous current modes of operation is a function of the magnetizing inductance,  $L_m$ . This is shown in Fig. 9.

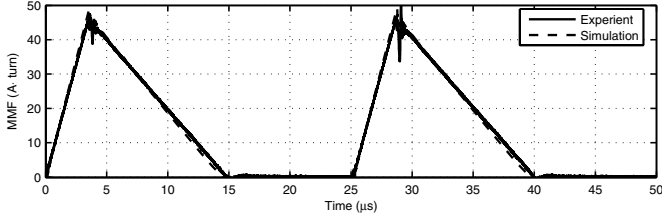


Fig. 9. Experimental and simulated MMF, Slope  $\propto \frac{1}{L_m}$

The triple-output converter, as with a single-output flyback converter, also has a triangular MMF waveform as seen in Fig. 9. The MMF obtained for all the simulations in Fig. 7 and Fig. 8 are in perfect agreement with the experimental MMF. Additionally, the rising and falling slope of the MMF waveform is inversely proportional to the magnetizing inductance,  $L_m$ , which is the same for all the equivalent circuits. Therefore, the boundary between continuous and discontinuous mode of operation depends on the magnetizing inductance. An ideal transformer with the correct magnetizing inductance will correctly predict the boundary between continuous and discontinuous current modes of operation for a multi-output flyback converter.

### C. Shapes of waveforms

As shown in Fig. 8(d) and Fig. 8(e), the inductances affect the shapes of the waveforms although the change in an inductance should be considerable in order to introduce a visible change in the waveforms, e.g. a 50% change in  $L_{44}$ .

Fig. 8(f) shows that the shapes of the waveforms are extremely sensitive to coupling factors. A change even as small as 1% in a coupling factor has a significant impact on the shapes of the waveforms. This implies that even small errors in estimating coupling factors can introduce large discrepancies between the simulated and experimental shapes of the waveforms for the flyback converter.

Equation (8), which is obtained from (7), is used to acquire an estimate of the coupling factor variation  $\Delta k_{ij}$  with respect to the variations of the inductances.

$$\begin{aligned} \Delta k_{ij} = & \frac{\partial k_{ij}}{\partial L_i} \Delta L_i + \frac{\partial k_{ij}}{\partial L_{ser_i}} \Delta L_{ser_i} \\ & + \frac{\partial k_{ij}}{\partial L_j} \Delta L_j + \frac{\partial k_{ij}}{\partial L_{ser_j}} \Delta L_{ser_j} + \frac{\partial k_{ij}}{\partial L_{ser_{ij}}} \Delta L_{ser_{ij}} \end{aligned} \quad (8)$$

As an example, (8) is applied to compute  $\Delta k_{14}$  as follows:

$$\begin{aligned} \Delta k_{14} = & 0.002 \Delta L_1 \% - 0.080 \Delta L_{ser_1} \% \\ & + 0.006 \Delta L_4 \% - 0.084 \Delta L_{ser_4} \% + 0.156 \Delta L_{ser_{14}} \% \\ \therefore |\Delta L' s| \leq 10\% \Rightarrow & |\Delta k_{14}| \leq 3\%. \end{aligned} \quad (9)$$

The above equation shows that the cumulative errors of the inductances can lead to an unacceptable error in the coupling factor. For example, a typical error of 10% in determining the inductances implies that the coupling factor  $k_{14}$  can have an error of up to 3%. This leads to a substantial change in

waveforms. Therefore, the coupled inductances, e.g.  $L_1$  and  $L_4$  and series inductances in the Foster networks, e.g.  $L_{ser_1}$  and  $L_{ser_{14}}$ , have to be obtained with the smallest errors possible in order to decrease the errors in the coupling factors.

Equations (7) and (8) also show that the coupling factors are not changed by the shunt inductances of the Foster networks, e.g.  $L_{par_1}$  and  $L_{par_{12}}$  in Fig 1. Furthermore, Fig 8(e) illustrates that eliminating all of the parallel RL branches in the Foster networks does not result in a significant impact on the waveforms. Thus, it seems that the order of the Foster networks have no impact on the coupling factors. However, one should note that the use of higher order Foster networks results in an improved agreement between the frequency responses of the Foster networks and the FEM results. Thus the series inductances and consequently the coupling factors are calculated with lower errors. In other words, shunt inductances and the order of the Foster networks has indirect effects on the coupling factors.

Another conclusion from (8) is that simulations with a reduced-order network, such as the one used in [1], generally cannot replicate the secondary current waveform of a multi-output flyback converter. The removal of leakage inductances results in large errors in the coupling factors and large discrepancies between simulated and experimental waveforms. The experimental results presented in [1] justify this argument.

## V. FREQUENCY DEPENDENCY OF COUPLING FACTORS

PEmag can also be used to develop a magnetic component's equivalent circuit just for a single frequency instead of a range of frequencies. Modeling the coupled inductor case study was carried out for single frequencies ranging from 100 kHz to 2.5 MHz and the coupling factors for each frequency were calculated. The resistances and inductances of the equivalent network and also the coupling factors are dependent on frequency. With increasing frequency, the coupling factors increase. As an example, the coupling factors rise by less than 1.2% when the frequency increases from 100 kHz to 1 MHz. This change is substantial and can change the shapes of the waveforms. Consequently, the high frequency effects generated by switch transitions are also important in determining the waveform shapes.

The effects of using a wider range of frequencies for modeling using PEmag are also examined. The equivalent network of the coupled inductor is obtained over a frequency range from DC to 2 MHz, which is twice the range that was used previously, i.e. DC to 1 MHz. The simulation results are shown in Fig. 10. Comparing Fig. 10 with Fig. 8(b) reveals that there is no substantial improvement in the waveforms in terms of being in better agreement with the experimental results. The reason is that the network model for the wider frequency range has been obtained with larger errors (by about 10%) in its Foster networks with respect to those of the model with the smaller frequency range. The orders of the Foster networks in PEmag are fixed and cannot be increased by the user in order to lower the errors.

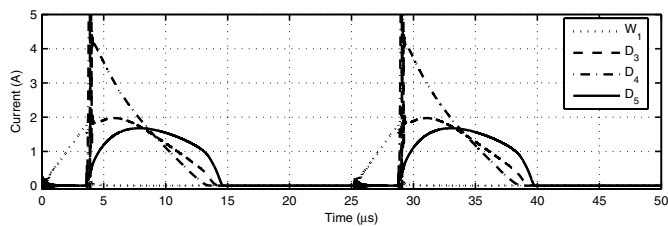


Fig. 10. Current waveforms of a 0–2 MHz equivalent circuit

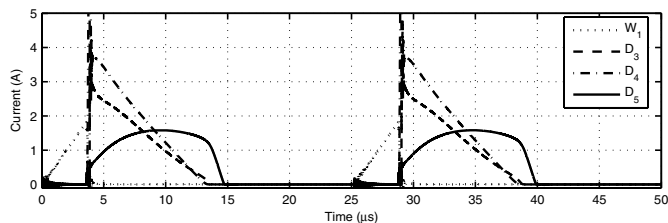


Fig. 11. Current waveforms of model obtained for loosely wound coupled inductor w.r.t. Fig. 8(b)

## VI. EFFECTS OF WINDING STRATEGIES

In developing the circuit model for the coupled inductor using PEmag, we assumed that the turns in each winding layer are tightly wound together and layers are separated by a distance of 0.6 mm. Intuitively, if the turns are wound loosely, leakage will be larger resulting in changes to the coupling factors. To study the impacts that this may have on the waveforms, an additional winding strategy is modeled in which the the distance between adjacent winding turns in each layer and the distance between adjacent layers are increased to 0.25 and 1 mm respectively. The range of frequencies for this strategy is DC to 1 MHz, the same as was used for generating the data in Fig 8. The coupling factors decrease from those of the tightly wound strategy by up to 3% which implies large differences in the waveforms, as illustrated in Fig. 11. Therefore, the winding strategy should also be taken into account in modeling a magnetic component for a multi-output flyback converter. Another implication of the above discussion is that when the coupled inductor is wound, the tolerances in winding placement can have an impact on the coupling factors which in turn changes the secondary current waveforms.

## VII. CONCLUSIONS

PEmag was used to obtain an equivalent circuit for a coupled inductor that operates in a triple-output flyback converter. An alternative circuit was formulated from the PEmag circuit which not only overcomes convergence problems but also improves the simulation run time and/or accuracy of the solution. Effects of the circuit parameters on the simulated waveforms were studied. It was found that the values of the resistances and J–A parameters in the equivalent circuit have no substantial effects on the waveform shapes. In addition, the boundary between continuous and discontinuous current

modes of operation for a multi-output flyback converter depends on the magnetizing inductance only. It was also shown that the key to having a good agreement between simulated and experimental secondary current waveforms is to have very accurate estimates of the coupling factors. Small deviations in the coupling factors can significantly change the shape of the waveforms. Therefore, no reduced order model can accurately replicate the waveforms. Moreover, the coupling factors depend on the frequency. Therefore, the high frequency effects generated by switch transitions are also important in determining the waveform shapes. It was also found that the winding strategy is influential in determining the coupling factors and waveforms. Loosely wound windings have smaller coupling factors than those which are tightly wound.

## ACKNOWLEDGMENT

The authors wish to express their gratitude to Professor P. Jain and Mr. D. Hamza from Queen’s University and Professor A. Prodic, Professor P. Lehn, Mr. J. Goldstein and Mr. M. Mehramiz from the University of Toronto for kindly providing help and the experimental facilities.

## REFERENCES

- [1] K. Changtong, R. Erickson, and D. Maksimovic, “A comparison of the ladder and full-order magnetic models,” in *PESC '01. 32nd Annual IEEE*, vol. 4, June 2001, pp. 2067–2071.
- [2] *PEmag Reference Manuals*, Ansoft Corp., 2001.
- [3] R. Prieto, L. Ostergaard, J. Cobos, and J. Uceda, “Axisymmetric modeling of 3D magnetic components,” in *APEC '99. 14th Annual IEEE*, vol. 1, March 1999, pp. 213–219.
- [4] R. Prieto, R. Asensi, J. Cobos, O. Garcia, and J. Uceda, “Model of the capacitive effects in magnetic components,” in *PESC '95. 26th Annual IEEE*, vol. 2, June 1995, pp. 678–683.
- [5] J. Lavers and E. Lavers, “An accuracy assessment of 2–D vs. 3–D finite element models for ferrite core, sheet wound transformers,” in *APEC '02. 17th Annual IEEE*, vol. 1, March 2002, pp. 158–164.
- [6] T. Sato and Y. Sakaki, “Physical meaning of equivalent loss resistance of magnetic cores,” *IEEE Transactions on Magnetics*, vol. 26, no. 5, pp. 2894–2897, Sep. 1990.
- [7] M. Albach, T. Durbaum, and A. Brockmeyer, “Calculating core losses in transformers for arbitrary magnetizing currents a comparison of different approaches,” in *PESC '96. 27th Annual IEEE*, vol. 2, June 1996, pp. 1463–1468.
- [8] K. Venkatachalam, C. R. Sullivan, T. Abdallah, and H. Tacca, “Accurate prediction of ferrite core loss with nonsinusoidal waveforms using only steinmetz parameters,” in *Proc. Workshop on Computers in Power Electronics. IEEE*, June 2002, pp. 36–41.
- [9] D. C. Jiles and D. L. Atherton, “Theory of ferromagnetic hysteresis,” *J. Appl. Phys.*, vol. 5, no. 6, pp. 2115–2120, 1984.